A&A 551, L6 (2013)
DOI: 10.1051/0004-6361/201220923

Astronomy & Astrophysics

Letter to the Editor

Accretion disk wind as explanation for the broad-line region structure in NGC 5548

W. Kollatschny and M. Zetzl

Institut für Astrophysik, Universität Göttingen, Friedrich-Hund Platz 1, 37077 Göttingen, Germany
e-mail: wkollat@astro.physik.uni-goettingen.de

Received 14 December 2012 / Accepted 26 January 2013

ABSTRACT

Context. Supermassive black holes in the centers of active galactic nuclei (AGN) are surrounded by broad-line regions (BLRs). The broad emission lines seen in the AGN spectra are emitted in this spatially unresolved region.
Aims. We intend to obtain information on the structure and geometry of this BLR based on observed line profiles.
Methods. We modeled the rotational and turbulent velocities in the line-emitting region on the basis of the line-width FWHM and line dispersion $\sigma_{\rm line}$ of the variable broad emission lines in NGC 5548. Based on these velocities we estimated the height of the line-emitting regions above the midplane in the context of their distances from the center.
Results. The broad emission lines originate at distances of 2 to 27 light days from the center. Higher ionized lines originate in the inner region ($\leq$13 light days) in specific filamentary structures 1 to 14 light days above the midplane. In contrast, the Hβ line is emitted in an outer (6−26 light days), more flattened configuration at heights of 0.7 to 4 light days only above the midplane.
Conclusions. The derived geometry of the line-emitting region in NGC 5548 is consistent with an outflowing wind launched from an accretion disk.

Key words. accretion, accretion disks – line: profiles – galaxies: active – galaxies: Seyfert – galaxies: individual: NGC 5548 – quasars: emission lines

1. Introduction

It is now generally accepted that active galactic nuclei (AGN) are powered by accretion onto a super-massive black hole. The broad emission lines we observe in the UV/optical regime are generated by photoionization in the outer regions of an accretion disk that surrounds the central black hole. Many details of this line-emitting region are unknown. The broad-line region with an extension of about ten light days is spatially unresolved on direct images. However, some basic information about the distances of the line-emitting regions from the central ionizing region can be obtained from reverberation mapping (e.g. Clavel et al. 1991; Peterson et al. 2004), i.e., the delayed variability of the integrated emission lines with respect to that of the ionizing continuum. Furthermore, there is stratification in the broad-line region. The higher ionized lines originate closer to the central ionizing source than the lower ionized lines. In a few cases the individual delays of emission line segments (velocity delay maps) could be studied. Comparing these velocity delay maps with model calculations point to the existence of accretion disks with additional signatures of accretion disk winds (Kollatschny 2003; Bentz et al. 2010).

Little is known about the size and geometry of the broad-line region perpendicular to the accretion disk. There are many models dealing with the geometry and structure of accretion disks in AGN, as well as accretion disk winds (e.g. Blandford 1982; Collin-Souffrin et al. 1988; Emmering et al. 1992; Königl & Kartje 1994; DeKool & Begelman 1995; Murray & Chiang 1997, 1998; Bottorff et al. 1997; Blandford & Begelman 1999; Elvis 2000; Proga et al. 2000; Proga & Kallman 2004; Kollatschny 2003, 2013; Ho 2008; Goad et al. 2012, and references therein). The origin of an accretion disk winds is explained by radiation-driven winds or magnetocentrifugal winds.

We have demonstrated in two recent papers (Kollatschny & Zetzl 2011, hereafter Paper I; and Kollatschny & Zetzl 2013, hereafter Paper II) that general relations exist between the full-width at half maximum (FWHM) and the line-width ratio FWHM/$\sigma_{\rm line}$ in the broad emission lines of AGN. The line-width FWHM reflects the rotational motion of the broad-line gas in combination with an associated turbulent motion. This turbulent velocity is different for the different emission lines. The rotational and turbulent velocities give us information on the accretion disk height with respect to the accretion disk radius of the line-emitting regions. We know the absolute numbers of the line-emitting radii from reverberation mapping, so we can get information on the absolute heights of the line-emitting regions above the accretion disks. Here we present results for the broad-line region geometry of NGC 5548.

2. The NGC 5548 data sample

One of the most extensive studied Seyfert galaxies is NGC 5548. The spectra of the broad optical emission lines, including the Hβ line, have been monitored over more than ten years by large international collaborations (e.g. Peterson et al. 2002, and references therein).

Furthermore, two additional campaigns have been carried out in combination with the IUE and HST satellites. In a first combined optical/UV variability campaign NGC 5548 was monitored with the IUE satellite for a period of eight months from 1988 December until 1989 August (Clavel et al. 1991), as well as in the optical from 1988 December until 1989 October (Peterson et al. 1991). In a second combined optical/UV variability campaign NGC 5548 was monitored with the IUE and HST, along with ground-based telescopes, for a period from 1992 October until 1993 September (Korista et al. 1995).

Table 1. Line profile parameters and the line-emitting regions of the individual emission lines.

Line	*FWHM* [km s^{-1}]	*FWHM*/σ	$v_{\rm turb}$ [km s^{-1}]	$v_{\rm rot}$ [km s^{-1}]	Radius [ld]	Height [ld]	H/R	Height$_{\rm corr}$ [ld]	$H_{\rm corr}/R$
NGC 5548–1988/1989 (opt+IUE)									
He II λ1640	9803 ± 1594	2.516 ± 0.130	1943^{+1763}_{-1383}	5700^{+974}_{-1356}	$3.8^{+1.7}_{-1.8}$	1.3 ± 1.4	0.34	1.5 ± 1.4	0.39
He II λ4686	7338 ± 901	2.575 ± 0.103	928^{+573}_{-536}	4297^{+528}_{-579}	$7.8^{+3.2}_{-3.0}$	1.7 ± 1.3	0.22	1.6 ± 1.3	0.21
C IV λ1549	6556 ± 878	1.706 ± 0.076	3537^{+1256}_{-1050}	3263^{+901}_{-1492}	$9.8^{+1.9}_{-1.5}$	10.6 ± 6.5	1.08	8.7 ± 5.7	0.89
Si IV λ1400	6455 ± 3030	2.506 ± 0.288	807^{+1489}_{-10806}	3780^{+1737}_{-2287}	$12.3^{+3.4}_{-3.0}$	2.6 ± 35.2	0.21	6.8 ± 35.5	0.55
Hβ	4044 ± 199	2.397 ± 0.061	374^{+86}_{-85}	2368^{+116}_{-117}	$19.7^{+1.5}_{-1.5}$	3.1 ± 0.8	0.16	3.3 ± 0.8	0.17
C III] λ1909	5018 ± 1458	2.126 ± 0.156	907^{+657}_{-646}	2925^{+867}_{-1028}	$27.4^{+5.4}_{-5.3}$	8.5 ± 7.0	0.31	14.1 ± 8.4	0.51
NGC 5548–1992/1993 (opt+IUE+HST)									
He II λ1640	8929 ± 1571	2.031 ± 0.056	4137^{+2222}_{-1662}	4691^{+1370}_{-2539}	$1.9^{+0.3}_{-0.3}$	1.7 ± 1.3	0.89	0.9 ± 1.0	0.47
Si IV λ1400	7044 ± 1849	1.755 ± 0.090	3878^{+6121}_{-1789}	3474^{+1661}_{-2429}	$4.3^{+1.1}_{-1.0}$	4.8 ± 8.4	1.12	2.6 ± 7.8	0.60
C IV λ1549	6868 ± 450	2.064 ± 0.051	2002^{+426}_{-400}	3906^{+333}_{-377}	$6.7^{+0.9}_{-1.0}$	3.4 ± 1.0	0.51	5.0 ± 1.1	0.75
Hβ	7202 ± 392	2.488 ± 0.075	1048^{+336}_{-316}	4213^{+235}_{-257}	$13.4^{+3.8}_{-4.3}$	3.3 ± 1.5	0.25	1.3 ± 1.1	0.10
C III] λ1909	4895 ± 1263	1.517 ± 0.070	2488^{+811}_{-796}	2495^{+1024}_{-1615}	$13.9^{+1.8}_{-1.4}$	13.9 ± 10.2	1.00	8.4 ± 7.1	0.60
NGC 5548–Hβ									
Hβ	5957 ± 224	3.025 ± 0.055	223^{+104}_{-102}	3468^{+129}_{-128}	$6.5^{+5.7}_{-3.7}$	0.4 ± 0.4	0.06	0.7 ± 0.7	0.11
Hβ	8047 ± 1268	2.614 ± 0.127	1043^{+879}_{-792}	4711^{+743}_{-847}	$7.8^{+3.8}_{-2.8}$	1.7 ± 1.7	0.22	0.7 ± 1.5	0.09
Hβ	5691 ± 164	2.514 ± 0.074	614^{+153}_{-146}	3333^{+96}_{-99}	$11.0^{+1.9}_{-2.0}$	2.0 ± 0.6	0.18	1.3 ± 0.6	0.12
Hβ	7202 ± 392	2.488 ± 0.075	1048^{+336}_{-316}	4213^{+235}_{-257}	$13.4^{+3.8}_{-4.3}$	3.3 ± 1.5	0.25	1.3 ± 1.1	0.10
Hβ	6247 ± 343	2.875 ± 0.088	361^{+194}_{-187}	3648^{+199}_{-200}	$14.3^{+5.9}_{-7.3}$	1.4 ± 1.1	0.10	1.6 ± 1.1	0.11
Hβ	5776 ± 237	2.784 ± 0.082	377^{+149}_{-143}	3376^{+139}_{-140}	$15.9^{+2.9}_{-2.5}$	1.8 ± 0.8	0.11	1.9 ± 0.8	0.12
Hβ	5706 ± 357	2.816 ± 0.071	343^{+160}_{-157}	3333^{+206}_{-206}	$16.4^{+1.2}_{-1.1}$	1.7 ± 0.8	0.10	2.0 ± 0.8	0.12
Hβ	5541 ± 354	2.881 ± 0.070	280^{+144}_{-143}	3233^{+202}_{-204}	$17.5^{+2.0}_{-1.6}$	1.5 ± 0.8	0.09	2.2 ± 0.8	0.13
Hβ	4664 ± 324	2.478 ± 0.083	435^{+152}_{-147}	2731^{+189}_{-191}	$18.6^{+2.1}_{-2.3}$	3.0 ± 1.1	0.16	2.7 ± 1.1	0.15
Hβ	4044 ± 199	2.397 ± 0.061	374^{+86}_{-85}	2368^{+116}_{-117}	$19.7^{+1.5}_{-1.5}$	3.1 ± 0.8	0.16	3.3 ± 0.8	0.17
Hβ	6142 ± 289	2.733 ± 0.123	473^{+244}_{-226}	3593^{+171}_{-172}	$21.7^{+2.6}_{-2.6}$	2.9 ± 1.5	0.13	2.4 ± 1.5	0.11
Hβ	6377 ± 147	3.221 ± 0.036	127^{+67}_{-67}	3700^{+84}_{-84}	$24.8^{+3.2}_{-3.0}$	0.9 ± 0.5	0.04	2.7 ± 0.6	0.11
Hβ	4596 ± 505	2.654 ± 0.088	309^{+168}_{-169}	2686^{+291}_{-292}	$26.5^{+4.3}_{-2.2}$	3.0 ± 1.8	0.11	3.9 ± 1.8	0.15

Our current investigation is based on all spectral information of the root-mean-square (rms) emission line profiles in NGC 5548 (Peterson et al. 2004). The narrow line components disappear in these spectra. This sample has been the basis for our Papers I and II as well.

Altogether, we have information about the rms line profile widths FWHM and $\sigma_{\rm line}$, along with distances of the emitting regions from the central ionizing source for the following emission lines: the optical Hβ and He II λ4686 lines, and the UV He II λ1640, C III] λ1909, C IV λ1550, and S IV λ1400 lines (see Table 1). For the Hβ line we know their annual rms profiles over a period of 14 years (1988−2001) and their related distances. For the He II λ4686 line we only know one rms profile based on the campaign in 1988/1989. However, for the rest of the UV lines we have two rms profiles based on the campaigns in the years 1988/89 and 1992/93.

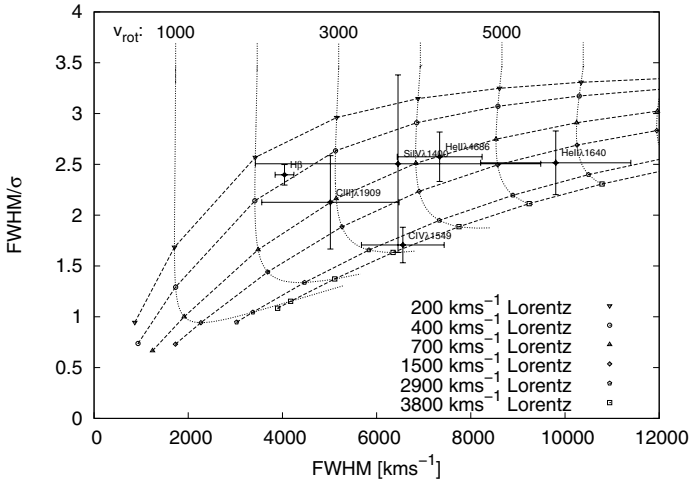

Fig. 1. NGC 5548: Observed and modeled line-width ratios FWHM/$\sigma_{\rm line}$ versus line-width FWHM for the period 1988/89.

3. Results

3.1. Observed and modeled emission line-width ratios

We parameterize the rms line profiles by both their FWHM and the ratio of their FWHM to their line dispersion $\sigma_{\rm line}$. We present in Table 1 and Figs. 1 to 3 the observed line widths of the emission lines in NGC 5548, the corresponding modeled turbulent $v_{\rm turb}$, and rotational velocities $v_{\rm rot}$ of the line-emitting regions (see Papers I, II). The $\sigma_{\rm line}$ values of the modeled profiles are integrated over line-widths 25 000 km s^{-1} (see Paper I). The modeled line-width ratios FWHM/$\sigma_{\rm line}$, hence the turbulent velocities, would decrease/increase by 10−20 percent if we integrated over line-widths that are broader/smaller by 20 percent. However, the general trends remain the same.

The observed and modeled line-width ratio FWHM/$\sigma_{\rm line}$ versus line-width FWHM are presented separately for the two variability campaigns of the years 1988/89 and 1992/93, as well as

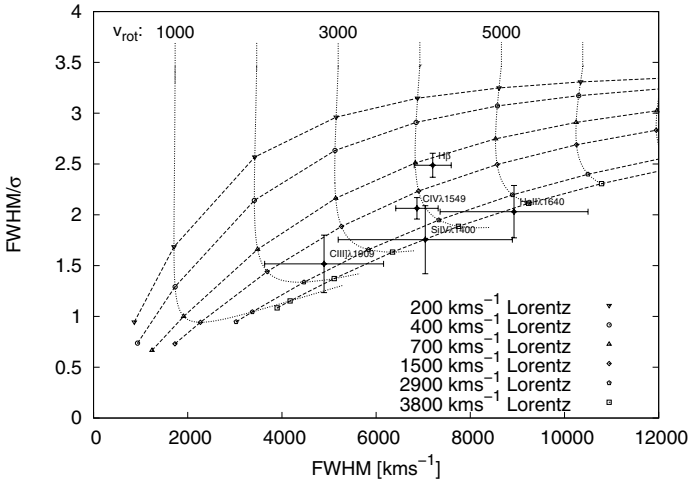

Fig. 2. NGC 5548: observed and modeled line-width ratios FWHM/$\sigma_{\rm line}$ versus line-width FWHM for the period 1992/93.

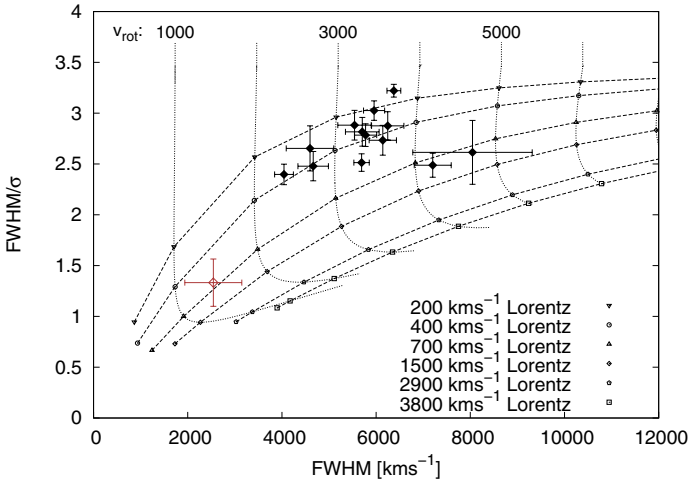

Fig. 3. NGC 5548: observed and modeled Hβ line-width ratios FWHM/$\sigma_{\rm line}$ versus line-width FWHM over 14 years (1988−2001).

for the 14 Hβ rms lines based on their annual profiles for the years 1988 until 2001. One Hβ rms profile strongly deviates from the Hβ profiles of the other years in Fig. 3 (red cross at $FWHM = 2500\,{\rm km\,s^{-1}}$). This profile has been considered to be less reliable by Peterson et al. (2004) before. We neglect this individual profile for the rest of our investigation.

The ratio of the turbulent velocity $v_{\rm turb}$ over the rotational velocity $v_{\rm rot}$ in the line-emitting region gives us information on the ratio of the accretion disk height H with respect to the accretion disk radius R of the line-emitting regions as presented in Papers I and II:

$$H/R = (1/\alpha)(v_{\rm turb}/v_{\rm rot}). \quad (1)$$

The unknown viscosity parameter α is assumed to be constant and to have a value of one. In reality, the value of α might be up to one order lower.

Since we know the distances R of the line-emitting regions from reverberation mapping (Table 1), we are able to estimate the height H of the line-emitting region. We present in Table 1 information on both the height of the line-emitting region in units of light days and the ratio H/R.

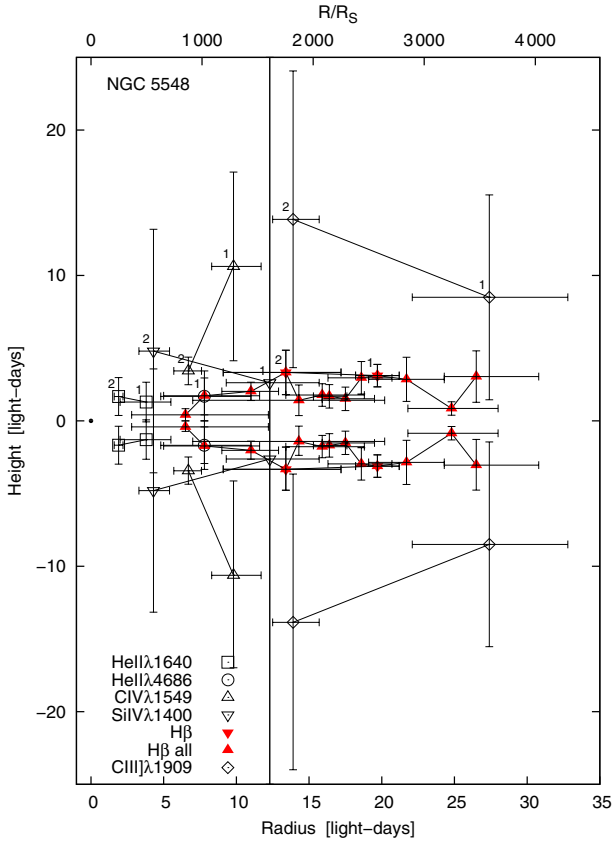

Fig. 4. Broad-line region structures of NGC 5548 based on the dominant emitting regions of the broad optical/UV lines as a function of distance to the center and of height above the midplane. The emission regions of the individual lines that are observed at different epochs are connected by a solid line. The dot at radius zero gives the size of a Schwarzschild black hole (with $M = 6.7 \times 10^7\ M_\odot$) multiplied by a factor of twenty.

3.2. Broad-line region geometry of NGC 5548

The broad-line region structure of NGC 5548 based on the radius and height data in Table 1 is shown in Fig. 4. Given are the emitting regions of the He II λ1640, Si IV λ1400, C IV λ1550, C III] λ1909, as well as Hβ rms emission lines (red symbols) as a function of distance to the center and of the height above the midplane for the two epochs 1988/89 (1) and 1992/93 (2). Furthermore, the position of the Hβ emitting region is presented for all 13 rms spectra obtained for the years 1988 to 2001 (Hβ all). The He II λ4686 line has only been monitored at one epoch. The dot at radius zero gives the size of a Schwarzschild black hole (with $M = 6.7 \times 10^7\ M_\odot$) multiplied by a factor of twenty. The two axes' scale in Fig. 4 are linear in units of light days. One light day corresponds to a distance of 2.59×10^{15} cm. The axis on top of the figure gives the distance of the line-emitting regions from the center in units of the Schwarzschild radius (for a central black hole mass of $M = 6.7 \times 10^7\ M_\odot$ taken from Peterson et al. 2004). We make the assumption that the accretion disk structure is arranged symmetrically to the midplane in Figs. 4 and 5.

The errors of the line widths (in Table 1) and therefore of the derived turbulent velocities $v_{\rm turb}$ are quite large for the weak UV emission lines in NGC 5548. This especially applies to the Si IV λ1400 and C III] λ1909 line profiles based on IUE spectra. We demonstrated in Papers I and II that dedicated turbulent velocities belong to the individual emission line regions. These dedicated velocities have been derived from many line profiles. Therefore, we then calculated additional corrected heights of

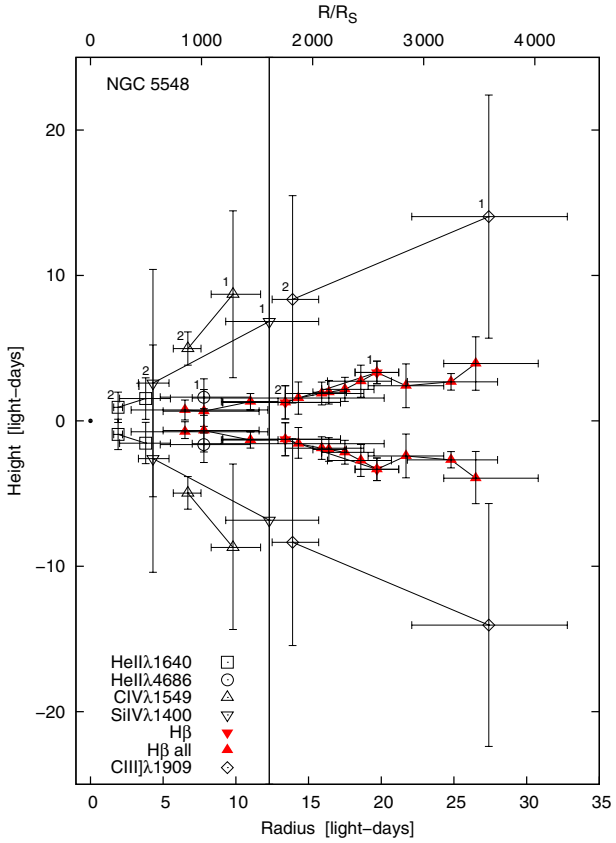

Fig. 5. Broad-line region structure of NGC 5548 based on the dominant emitting regions of the broad optical/UV lines as a function of distance to the center as well as height above the midplane. This figure is based on corrected turbulent velocities $v_{\rm turb}$. The dot at radius zero gives the size of a Schwarzschild black hole (with $M = 6.7 \times 10^7\ M_\odot$) multiplied by a factor of twenty.

the line-emitting regions based on the turbulent velocities belonging to the individual lines (see Papers I, II): 400 km s^{-1} for Hβ, 900 km s^{-1} for He II λ4686, 1500 km s^{-1} for C III] λ1909, 2100 km s^{-1} for Si IV λ1400, 2300 km s^{-1} for He II λ1640, and 2900 km s^{-1} for C IV λ1549. We give in Table 1 the corrected height Height$_{\rm corr}$ of the line-emitting regions based on these $v_{\rm turb}$. The broad-line region structure of NGC 5548 based on the corrected turbulent velocities $v_{\rm turb}$ is shown in Fig. 5.

The radius of the dominating Hβ line-emitting region varied by a factor of more than four during the monitoring campaign from the year 1988 until 2001. It has been shown before that the distances of the line-emitting regions depend on the luminosity of the central ionizing source (e.g. Dietrich & Kollatschny 1995; Peterson et al. 2002, 2004). It should be emphasized that the individual emission lines do not originate at one single radius only, but rather in an extended region (see e.g. Kollatschny 2003). Therefore it is reasonable to connect the individual line-emitting regions as shown in Figs. 4 and 5. Furthermore, it was known before that higher ionized lines originate closer to the central ionizing source as seen in Fig. 5. The C IV λ1549 line, e.g., originates inwards of the C III] λ1909 line.

The Hβ lines are emitted in a more flattened configuration above the midplane. The Hβ line originates at a height of 0.7 light days only at a radius of seven light days. This corresponds to theoretical H/R values of 0.01–0.3 (e.g. DeKool & Begelman 1995) based on accretion disk models. However, the higher ionized lines in NGC 5548 originate in a far more extended region above the presumed accretion disk. We observe H/R values of 0.1 until 0.9 (Table 1, Fig. 5) for the line-emitting regions. This indicates that the emission lines do not originate in a thin atmosphere of an accretion disk but rather in filaments at greater heights above the disk. The different geometries of the high/low ionization lines might be explained by a nonspherical geometry of the photoionizing source.

The observed geometry of the BLR in NGC 5548 strikingly corresponds to the disk wind models of Murray & Chiang (1997, their Fig. 1) and Proga & Kallman (2004, their Fig. 1d). Furthermore, the emitting region of the Hβ line is arranged more horizontally in comparison to the higher ionized lines. It has been predicted by Murray & Chiang (1997) in their models that the angle the streamlines make with the disk vary with the distance/radius of the footprint of the streamline. The streamlines – based on their model – should be more vertical at smaller radii, as seen in Fig. 5.

4. Conclusions

We demonstrate in our investigation that the higher ionized lines of the broad-line region originate in an extended region of 1 to 14 light days above the midplane. In contrast, the Hβ line only originates at distances of 0.7 to 4 light days above the midplane. The derived filamentary geometry of the broad-line emitting region in NGC 5548 is consistent with models of an outflowing wind launched from an accretion disk.

Acknowledgements. Part of this work was supported by the German *Deutsche Forschungsgemeinschaft, DFG* project number Ko 857/32-1.

References

Bentz, M. C., Horne, K., Barth, A. J., et al. 2010, ApJ, 720, L46
Blandford, R. D., & Payne, D. G. 1982, MNRAS, 199, 883
Blandford, R. D., & Begelman, M. C. 1999, MNRAS, 303, L1
Bottorff, M., Korista, K. I., Shlosman, I., et al. 1997, ApJ, 479, 200
Clavel, J., Reichert, G. A., Alloin, D., et al. 1991, ApJ, 366, 64
Collin-Souffrin, S., Dyson, J. E., McDowell, J. C., & Perry, J. J. 1988, MNRAS, 232, 539
Collin, S., Kawaguchi, T., Peterson, B. M., & Vestergaard, M. 2006, A&A, 456, 75
DeKool, M., & Begelman, M. C. 1995, ApJ, 455, 448
Dietrich, M., & Kollatschny, W. 1995, A&A, 303, 405
Elvis, M. 2000, ApJ, 545, 63
Emmering, R. T., Blandford, R. D., & Shlosman, I. 1992, ApJ, 385, 460
Goad, M. R., Korista, K. T., & Ruff, A. J. 2012, MNRAS, 426, 3086
Ho, L. 2008, ARA&A, 45, 475
Königl, A., & Kartje, J. E. 1994, ApJ, 434, 446
Kollatschny, W. 2003, A&A, 407, 461
Kollatschny, W., & Zetzl, M. 2011, Nature, 470, 366 (Paper I)
Kollatschny, W., & Zetzl, M. 2013, A&A, 549, A100 (Paper II)
Korista, K. T., Alloin, D., Barr, P., et al. 1995, ApJS, 97, 285
Murray, N., & Chiang, J. 1997, ApJ, 474, 91
Murray, N., & Chiang, J. 1998, ApJ, 494, 125
Peterson, B. M., Balonek, T. J., Barker, E. S., et al. 1991, ApJ, 368, 119
Peterson, B. M., Berlind, P., Bertram, R., et al. 2002, ApJ, 581, 197
Peterson, B. M., Ferrarese, L., Gilbert, K. M., et al. 2004, ApJ, 613, 682
Proga, D., & Kallman, T. R. 2004, ApJ, 616, 688
Proga, D., Stone, J. M., & Kallman, T. R. 2000, ApJ, 543, 686